Relativistic-consistent electron densities of the coinage metal clusters M2, M4, M4 2-, and M 4Na2 (M = Cu, Ag, Au): A QTAIM study

ARTICLE *in* THE JOURNAL OF PHYSICAL CHEMISTRY A · AUGUST 2011

Impact Factor: 2.69 · DOI: 10.1021/jp204993r · Source: PubMed

4 AUTHORS, INCLUDING:

Ian Hamilton
Wilfrid Laurier University
89 PUBLICATIONS **1,995** CITATIONS

Relativistic-Consistent Electron Densities of the Coinage Metal Clusters M_2, M_4, M_4^{2-}, M_4Na_2 (M = Cu, Ag, Au): A QTAIM Study

Abdolreza Sadjadi,[1] Chérif F. Matta,[2] Kono Lemke,[1] I. P. Hamilton[3]*

[1] *Department of Earth Sciences, Pokfulam Road, University of Hong Kong, Hong Kong, SAR, China.*

[2] *Department of Chemistry and Physics, Mount Saint Vincent University, Halifax, Nova Scotia, Canada B3M 2J6; and Department of Chemistry, Dalhousie University, Halifax, Nova Scotia, Canada B3H 4J3.*

[3] *Department of Chemistry, Wilfrid Laurier University, 75 University Avenue West, Waterloo, Ontario, Canada N2L 3C5.*

Email: ihamilton@wlu.ca, telephone: 519.884.0710 ext. 2669, Fax: 519.746.0677.

ABSTRACT

We employ second-order Møller-Plesset perturbation theory level in combination with recently developed pseudopotential-based correlation consistent basis sets to obtain accurate relativistic electron densities for small coinage metal clusters. Using calculated electron densities we employ Bader's quantum theory of atoms in molecules (QTAIM) to gain insights into the nature of metal-metal bonding in the clusters M_2, M_4, M_4^{2-}, M_4Na_2 (M = Cu, Ag, Au). For the simplest case of the metal dimer, M_2, we correlate the strength of the metal-metal bond with the value of the electron density at the bond critical point, the total energy density at the bond critical point, the sharing (delocalization) index, and the values of the two principle negative curvatures. We then consider changes to the metal-metal bonding and charge density distribution upon the addition of two metal atoms to form the metal tetramer, M_4, and then followed by the addition of an electron pair to form M_4^{2-} and finally followed by the addition of two alkali metal (sodium) ions to form M_4Na_2. Using topological properties of the electron density we present evidence for the existence of σ–aromaticity in Au_4^{2-}. We also report the existence of two nonnuclear attractors in the molecular graph of Cu_4^{2-} and large negative charge accumulation in the non-bonded Cu basins of this cluster.

INTRODUCTION

Ab-initio approaches in which the Schrödinger equation is solved to obtain the *N*–electron wavefunction, Ψ, are ubiquitous in computational quantum chemistry and remain essential for highly accurate quantum chemical calculations.[1,2] From Ψ the electron density, $\rho(\mathbf{r})$, can be obtained by integrating Ψ*Ψ over the coordinates of $N-1$ electrons and multiplying by N. The *N*–electron wavefunction is a complex dynamical variable and is not an observable, but from it all properties of the system can be calculated and the existence of chemical bonding can be predicted. However, insight into the nature of the chemical bonding is often lacking from ab-initio studies, although molecular orbital (MO) models have proven to be very useful in this regard.

Over the past few decades there has been a great deal of interest in density functional theory (DFT).[3,4] In this approach the electron density is, in principle, obtained directly. The electron density is a Dirac "*observable*",[5] as pointed out by Bader and Zou,[6] since it is a *real* (not complex) dynamical variable which is the expectation value of a linear Hermitian operator ($\hat{\rho}(\mathbf{r})$) the eigenstates of which form a complete set of coordinate states $|\mathbf{r}\rangle$. Dirac emphasized (on page 37 of his book) that not every observable can, in practice, be measured,[5] but the electron density is measurable, indirectly, through the Fourier synthesis of the structure factors obtained from X-ray diffraction. The modeling of experimental densities, especially when refined aspherically, has reached the accuracy necessary to study the subtle characteristics of the density in the bonding regions between atoms,[7,8] and not only near the nuclei as in the past.[7-9]

From the electron density all properties of the system can be calculated but insight into the nature of the chemical bonding is often lacking from density functional studies. In fact, it is *not* the task of DFT, *ab initio* approaches, or X-ray diffraction experiments to delve into the nature of the chemical bonding. This critical task was undertaken by Professor Richard F. W. Bader, to whom we dedicate this paper, and his achievement culminated in the quantum theory of atoms in molecules (QTAIM).[10-15]

Over the past few decades, due primarily to the efforts of Bader and coworkers,[10-15] methods have been developed, which provide a novel perspective of chemical bonding from the topological analysis of the electron density. Analyses of chemical bonding based on QTAIM and MO models are by no means exclusive. In fact, Cortés-Guzmán and Bader discussed the complementarity of QTAIM and MO models for the description of bonding in donor-acceptor

complexes.[13] It is assumed the reader has some familiarity with QTAIM since it has been extensively reviewed elsewhere, comprehensively by its principal developer,[12] at an introductory/pedagogical level,[14] and as a collection of independent research reviews.[15]

Metal-Metal Bonding in Transition Metals

It has been known for over a decade that QTAIM indices of atom-atom bonding must be refined when the bonding is between metal atoms and, in particular, transition metal atoms.[16] Whereas metal-metal bonds would be classified as closed-shell interactions, this is an oversimplification, particularly for open shell metal atoms where a degree of shared interaction (covalency) is expected.

The QTAIM picture of metal-metal bonding has been extensively examined in organometallic and inorganic compounds[17-22] and also in bulk metals[23-25] using both calculated and experimental electron densities. The shell-structure of isolated atoms (H - U) and singly positive ions (He - Ba, and Lu - Ra) in terms of the laplacian of the electron density has been studied for the first time by Sagar *et al*.[26] and, simultaneously, by Shi and Boyd (Li - Xe) in 1988.[27] For transition metals (such as Co, Ni and Fe) general conclusions are that, for both organometallic compounds and bulk metals, the bond critical point (BCP) electron density (ρ_{BCP}) is relatively low, the Laplacian of the electron density ($\nabla^2\rho_{BCP}$) is positive, and the electron density (ρ) is relatively flat in the valence region. This is reasonable because transition metal atoms are generally characterized by the diffuse valence density of their outermost '*s*' electrons. Another general result is that for metal dimers, the electron density at the bond critical point (and on the entire interatomic surface) is larger for transition metals than it is for alkaline metals.[9,16,17,28-31]

To the best of the authors' knowledge, there have been no QTAIM studies of metal-metal bonding for coinage metals (Cu, Ag, and Au) but, at least for copper, it is reasonable to assume that the general conclusions found for other transition metals will hold. For copper there have been several recent theoretical and experimental studies[32-34] on complexes with through-bridge Cu-Cu coupling. Here the primary interest has been on the magnetic properties of these systems, in which the Cu(II) ions may be either ferromagnetically or antiferromagnetically coupled. However, a recent QTAIM study of a complex for which the antiferromagnetic coupling was large,[32] indicated a lack of any direct Cu-Cu coupling. We are not aware of any corresponding

studies for silver or gold complexes.

Coinage Metal Clusters

Recently there has been considerable interest in coinage metal clusters- particularly gold clusters, which have been found to exhibit a number of unique optoelectronic properties.[35-37] This uniqueness of gold clusters can be attributed partly to the "lanthanide contraction" but primarily to the strength of the relativistic effects for Au.

Relativistic effects are significant for Ag and partially relevant for Cu but, using the contraction of the outermost '*s*' shell as a measure, Au is the most relativistic of all the stable elements.[35-37] As a result, in gold clusters the valence density of the '6*s*' electrons is not as diffuse as that of the outermost '*s*' electrons in silver or copper clusters. Consequently, the gap between the '6*s*' and '5*d*' electrons of gold is much smaller than that between the outermost '*s*' and '*d*' electrons of silver and copper. As a result of more facile hybridization between the outermost '*s*' and '*d*' orbitals, gold can exhibit a broader range of valence states and gold clusters can exhibit a wider range of structural isomers.

In this paper we undertake a QTAIM study of metal-metal bonding in the coinage metal clusters M_2, M_4, M_4^{2-}, M_4Na_2 (M = Cu, Ag, Au). Of these, the M_4^{2-}, M_4Na_2 and the related M_4Na^- species (where another alkali metal may be substituted for Na) have been a focus of a number of previous studies on metal aromaticity.[38,39]

CALCULATION DETAILS

Second-order Møller-Plesset perturbation theory with frozen-core, MP2(FC), has been applied for geometry optimization and frequency calculations on a suite of coinage metal clusters with the general stoichiometry M_2 ($D_{\infty h}$), M_4 (D_{2h}, planar), M_4^{2-} (D_{4h}, planar) and M_4Na_2 (D_{4h}), where M = Cu, Ag, Au. All clusters have been calculated in their closed-shell singlet state, a state known to be the ground-state for the M_2, M_4, M_4^{2-} and M_4Na_2.[38,40-45] (See Table S1 in Supplementary Material for a comparison between our calculated singlet and triplet state total energies.) The pseudopotential (PP) aug-cc-pVTZ-PP(*spdfg*) basis set was applied for the Cu, Ag and Au atoms and the aug-cc-pVTZ(*spdf*) basis set was used for the Na atom. While a formally non-relativistic pseudopotential is employed, it is known to account for relativistic effects empirically, in addition of being correlation consistent.[40,46] The total number of electrons

and the number of electrons which have been replaced by the PP for each element (total/PP) are: Cu = 29/10, Ag = 47/28, and Au = 79/60; *i.e.*, in each case 19 electrons are treated explicitly per coinage metal atom (note, 8 electrons are treated as core and 11 as valence electrons in our electronic structure calculations). In order to obtain a wavefunction from the MP2 calculation (which is an "energy correlation method") an effective correlated "relaxed" density matrix is calculated by a method termed Z–vector correction to the SCF density matrix.[47,48]

The use of densities obtained using a pseudopotential presents several problems for a topological analysis of the electron density: (a) the lack of nuclear maxima, and (b) the appearance of spurious topological features near the boundary of the core electrons replaced by the PP. To achieve a meaningful QTAIM analysis, these problems were avoided by employing an approximation recently developed by Keith and Frisch in which cores replaced by the PP are augmented *after* the molecular density (missing the cores) is obtained from the electronic structure calculation.[49] Thus, after completion of the quantum mechanical calculation, the molecular electron density was augmented with subshell spherical densities fitted to reproduce electron densities for the ground state free atoms.[49]

All electronic structure calculations were performed using Gaussian09–Rev.B01[50] and all QTAIM calculations were performed using AIMAll.[51]

RESULTS AND DISCUSSION

Geometries and Molecular graphs

Ball and stick representations of the calculated geometries of all 12 clusters are depicted in Fig. 1 and the corresponding molecular graphs are presented in Fig 2. The coinage metal atom dimers, M_2, are the smallest and also the simplest, and because these systems have (cylindrical) $D_{\infty h}$ symmetry, there is no charge transfer and the M atoms therefore have no numerical labels. The optimized bond lengths of all three M_2 clusters are in good agreement with the experimental values, the calculated lengths being systematically shorter by 0.021 Å in the cases of Cu_2 and Au_2, and by 0.038 Å in the case of Ag_2 (see Table 2). The calculated bond dissociation energies at 0 K, including the zero-point vibrational energy (ZPE) corrections, also compare well with the

experimental values, being lower by 1.8 kcal/mol as in the case of Cu_2 but higher by 3.3 kcal/mol for both Ag_2 and Au_2. The good agreement between these calculated and experimental values enhances our confidence in the reliability and quality of our calculations. The calculated geometries recover the experimental order of M–M distance: Ag–Ag > Au–Au > Cu–Cu.

The M_4 clusters have (planar) D_{2h} symmetry, whereby all the peripheral M–M bonds are symmetry–equivalent, and these systems exhibit two types of M atoms which are distinguished by the labels "1" and "2" in Figs. 1 and 2. The former indicates the M atom type that bonds to its partner diagonally across the plane of the cluster, while the latter refers to the M atom type which is further apart and does not share a bond path.

The M_4^{2-} clusters retain the symmetry from their neutral counterparts for copper and silver but the Au_4^{2-} cluster has a higher symmetry (D_{4h}) than its neutral counterpart. This higher symmetry for gold is the result of the equalization of the two diagonal inter-nuclear distances, thus in the Au_4^{2-} cluster the Au atoms have no numerical labels. The equalization in the Au_4^{2-} cluster is the extreme of a similar trend observed among the corresponding copper and silver clusters.

It can be seen from Fig. 1 and Table 3 that in Cu_4 the M2…M2 (non-bonded) diagonal is longer than the M1-M1 (bonded) diagonal by 1.918 Å, a value that shrinks to 1.558 Å in Cu_4^{2-} (the corresponding values for silver are 2.106 Å and 1.434 Å, respectively). Thus the gain of the electron pair tends to equalize the diagonal distances in these clusters and achieves this equalization completely in the case of gold, the corresponding values in this case being 1.994Å and 0 Å, respectively.

It can be seen from Table 4 that the Cu_4 cluster is the most compact with a volume of 837.6 a.u. ($bohr^3$, the atomic unit of volume), gaining 119.7 a.u. with the acquisition of an electron pair to a volume of 957.3 a.u. in Cu_4^{2-}. The gain of the electron pair has a more significant effect on silver, the volume of Ag_4 (999.0 a.u.) increasing by 334.1 a.u. to 1333.1 a.u. in Ag_4^{2-}. Gold shows intermediary behaviour, the volume of Au_4 (1019.5 a.u.) increasing by 290.6 a.u to 1310.1 a.u. in Au_4^{2-}.

The attachment of two sodium ions (from above and below the M_4 plane) to the M_4^{2-} clusters results in the formation of the electrically neutral composite clusters M_4Na_2 which have D_{4h} symmetry, the plane of the four M atoms being a perfect square with no bond path linking diagonal atoms. Hence in these species, all M atoms are equivalent (and both Na atoms are

equivalent as well) and the atoms therefore have no numerical labels. The copper composite cluster is significantly more compact with a total volume of 1168.3 a.u, compared to Ag_4Na_2 (volume = 1337.5 a.u.) or Au_4Na_2 (volume = 1300.8) (see Table 4).

All molecular graphs presented in Fig. 2 satisfy the Poincaré-Hopf (PH) relationship regarding the number and type of critical points (CP) in these clusters.[7,10]

$$n_{\mathrm{NCP}} + n_{\mathrm{NNA}} - n_{\mathrm{BCP}} + n_{\mathrm{RCP}} - n_{\mathrm{CCP}} = \begin{cases} 1 & \text{(Isolated molecules)} \\ 0 & \text{(Infinite crystals)} \end{cases}, \qquad (1)$$

where n is the number of the CP indicated in the subscript, NCP = nuclear critical point, NNA = non-nuclear attractor, BCP = bond critical point, RCP = ring critical point, CCP = cage critical point. Equation (1) yields unity for isolated systems, such as the clusters subject of this study, or 0 for periodic systems, in which case it is known as the Morse equation.[7] Satisfaction of the PH relationship indicates that the characteristic set of critical points is self-consistent but does not prove its completeness. For example, if both a BCP and an RCP are missed for a non-periodic system, $n_{\mathrm{NCP}} + n_{\mathrm{NNA}} - (n_{\mathrm{BCP}}-1) + (n_{\mathrm{RCP}}-1) - n_{\mathrm{CCP}} = 1$ is still satisfied.[14] In fact, eleven of the twelve molecular graphs depicted in Fig. 2 are complete, the exception being the Cu_4^{2-} cluster which exhibits a diffuse electron density and there exist two NNA's in the far diffuse area. Thus, while the molecular graph of the Cu_4^{2-} cluster in Fig. 2 is consistent, it is incomplete (as discussed below).

Cluster Energies

The total energies of all clusters, both "bottom of the well" values and values corrected by the addition of zero-point vibrational energies (ZPE), are listed in Table 1. The total energies, *per se*, are not very instructive, being an extensive (and hence, size-dependent) overall property of the system. When used to calculate binding energies and bond dissociation energies (BDE), these total energies become more chemically insightful. Unfortunately, the binding energy of the composite clusters of the type M_4Na_2 could not be calculated accurately as this would require mixing of two levels of theory (see footnote (c) of Table 1). To compare all M_n^x clusters on equal footing, we follow other authors[52] in calculating the binding energy per atom (see Table 1).

On going from M_2 to M_4, the binding energy per atom is more stabilizing for all coinage metals, *ca.* 11 kcal/mol for copper, *ca.* 9 kcal/mol for silver, and *ca.* 12 kcal/mol for gold. However, when the M_4 cluster gains an electron pair to form M_4^{2-}, the effect on the binding

energy per atom is entirely different. It is *destabilizing* for copper and silver, by *ca.* 8 kcal/mol and 4 kcal/mol, respectively, yet it is *stabilizing* for gold by *ca.* 5 kcal/mol. This additional stabilization of Au_4^{2-}, along with the observed equalization of the two diagonal distances, is indicative of aromatic stabilization of Au_4^{2-}. To confirm this prediction, it would be necessary to analyze the magnetically-perturbed wavefunction, and this may be the topic of a future study by us. Magnetically-perturbed wavefunctions can be used to compute NMR properties including the well-known NICS[53-55] aromaticity criterion due to Schleyer and co-workers,[38,56] and are also necessary for the subsequent QTAIM analysis of the atomic contributions to the magnetic shielding due to ring currents developed by Keith and Bader.[57-61]

In the case of the M_2 dimers, the binding energy per atom is just the negative of ½ of the bond dissociation energy. Only for these species do the BDE, the total binding energy, and the binding energy per atom all convey the same information. To underscore the strength of the chemical bonding in the M_2 dimers, we will use the BDE in the following discussion. Tables 1 and 2 show that there are significant differences in the BDEs of the M_2 dimers. The most strongly bound is the gold dimer- its BDE is 56.5(56.8) kcal/mol, a value that includes the ZPE correction (in parentheses is the "bottom of the well" value). The gold dimer is followed by the copper dimer (46.1(46.5) kcal/mol) and then by the silver dimer (41.1(41.4) kcal/mol). The range 41–57 kcal/mol falls in the grey area between the strongest hydrogen bonds (the energy of the hydrogen bond in $H^-...H–F$ is approximately 58 kcal/mol)[62] and weak non-polar covalent bonds such as the C–S bonds in dimethyl disulfide $CH_3(–)S–S–CH_3$ or ethyl methyl disulfide $C_2H_5(–)S–S–CH_3$ (*ca.* 56–57 kcal/mol),[63] or the weak C–C bond in 1,2,2,2–tertaphenylethane $PhCH_2(–)CPh_3$ (55 kcal/mol).[63]

Entries in Table 4 suggest that the bond strength in the dimers follows the sequence: Au–Au > Cu–Cu > Ag–Ag, the ρ_{BCP} values, total energy density at the BCP (H_{BCP}), and delocalization (electron pair sharing) index δ(M,M) are: Au–Au (0.093 a.u., –0.038 a.u., 1.188 shared pairs); Cu–Cu (0.073 a.u., –0.028 a.u., 1.152 shared pairs); and Ag–Ag (0.064 a.u., –0.019 a.u., 1.081 shared pairs). Thus the QTAIM bond descriptors are consistent with the experimental and calculated BDEs as listed in Table 2.

It is often mentioned in the QTAIM literature that ρ_{BCP} values provide a measure of bond order and bond strength, but plots of BDE versus ρ_{BCP} are seldom shown. This is understandable because, more often than not, the bonds described in this manner cannot be isolated without

breaking other parts of the molecule and, hence, BDE may not be definable in a straightforward manner. Further, the comparison often includes similar bonds, for example between the same elements. In this paper, a bold step is taken whereby the density at the bond critical point of dimers of *different* coinage metals is plotted against the calculated BDE in Fig. 3(a). The surprising result is the (very strong) linearity of the relationship, admittedly with only three data points, despite the fact that these are bonds between three different dimers. We have tested the correlation between the BDEs of the three M_2 dimers against all other bond properties listed in Table 3 and found three more particularly strong correlations: Fig. 3(b), an exponential relationship between the BDE and the sharing index, a mathematical form anticipated because of the exponential relation relating the sharing (delocalization) index and ρ_{BCP}, that is, $\delta(\Omega,\Omega')=\exp[A(\rho_{BCP} - B)]$, where A and B are constants;[64] Fig. 3(c), an almost linear relationship between the BDE and the total energy density at the BCP (H_{BCP}), a relationship reminiscent of the well-known Espinosa–Molins–Lecomte relation between the potential energy density at the BCP and the strength of hydrogen bonds;[65] Fig. 3(d), an almost linear relationship between the BDE and the value of the two principal negative curvatures, $\lambda_1 = \lambda_2$, which are equal due to cylindrical symmetry of the bond. It is important to note that there is no correspondingly straightforward correlation between the BDE and the bond lengths for the coinage metal dimers. These correlations suggest that one can indeed utilize ρ_{BCP} and H_{BCP} along with the delocalization index together to describe the strength of the bonding in the larger coinage metal clusters where the definition of a BDE is not unambiguous. The curvatures λ_1 and λ_2 are less straightforward to use as indicators of bond strength in other than cylindrically-symmetric bonds and, thus, will not be relied on to discuss the relative strength bonds in the larger coinage metal clusters.

Bond and Atomic Properties

The M–M bond in the M_2 clusters is significantly shorter than that in any of the larger clusters of the same coinage metal, indicating a higher bond order and strength. This is reflected in a higher ρ_{BCP}, H_{BCP} and $\delta(\Omega,\Omega')$ than any of the M–M bonds of the larger clusters of the same coinage metal (see Table 3). The QTAIM delocalization has been shown to provide an physically sound description of M−M bonding[18] since it varies continuously (rather than being an "all-or-none" descriptor of bonding as the bond path) and it provides an electron counting

accounting for the delocalization of electrons between every pairs of atoms in the molecule. In absence of charge transfer, a delocalization index[66] of value equal to unity, $\delta(\Omega,\Omega') = 1.0$, indicates that the number of electrons shared between the atomic basins Ω and Ω' is equal to one equally-shared pair. This index decreases with charge transfer which results in the unequal sharing of electrons such as that which occurs in ionic bonding.[66] Since in the M_2 clusters there is no inter-atomic transfer of charge, the sharing index can be taken to be equal to the bond order of the metal-metal bond. Hence, on the basis of the delocalization index, the bond orders of all metal-metal bonds are slightly greater than one: to one decimal, it is 1.2 for Au–Au and Cu–Cu, and 1.1 for Ag–Ag (see Table 3). Table 3 reveals that the two types of metal-metal bonding in M_4 are significantly weaker than in M_2, using any of the above three indicators of bond strength, namely, ρ_{BCP}, $\delta(\Omega,\Omega')$, or H_{BCP}. Generally the peripheral M1-M2 bondings in M_4 clusters are slightly weaker than M1-M1 diagonal bonding. The atoms in all M_4 are slightly polarized, M1 being positive with a net charge of *ca.* 0.2 a.u., transferred to M2, which bears an equal and opposite (negative) charge (see Tables 3, 4).

Figure 4 provides contour plots of the electron density and the associated gradient vector field in the planes of the metal atoms (plus one additional face of the bi-pyramid for the M_4Na_2) along with the zero-flux surface that partitions the total electron density in these clusters. The plots can be used to visually distinguish the shape of the different types of atoms of the same element in a complex. The first (top) panel in Fig. 4 shows the shape of the atomic basins in the M_2 cluster, which are clearly mirror images in each case, as required by symmetry. The situation is very different upon the addition of two metal atoms to form the M_4 cluster. The second panel shows the density in the molecular plane of the M_4 clusters, where one can visually distinguish the atoms M1 and M2. It may be seen that the atoms M1 are clearly smaller, (squeezed in between) two neighbouring M2 atoms, and this is confirmed by the atomic volumes listed in Table 4.

The situation is again very different upon the addition of an electron pair to form the M_4^{2-} cluster. Both the silver and gold clusters, when they receive the electron pair, distribute the excess charge close to evenly: (±0.5 a.u.) in the case of silver and (exactly) evenly in the case of gold. Interestingly, the diagonal Ag1-Ag1 bond has much less density at the BCP in Ag_4^{2-} (ρ_{BCP} = 0.029 a.u.) than in Ag_4 (0.056 a.u.), an indication of the weakening of this bond in the double anion, a conclusion supported by the values of H_{BCP} and δ(Ag1,Ag1) (see Table 3). In contrast,

the peripheral bond Ag1–Ag2 remains practically unchanged, albeit, exhibiting a slight increase in electron pair sharing. The non-bonded diagonal delocalization between the two Ag2 basins increases from 0.146 to 0.205, as the atoms become closer in space. In the case of gold, there is a catastrophic change of structure whereby the bond path Au1–Au1 vanishes, and there is no diagonal bond path in the double anion. The Au_4^{2-} cluster has again no inter-atomic charge transfer, all atoms bearing ¼ of the added charge, 0.5 electronic charge per atom. Hence the delocalization index is strictly a bond order and has the value of almost 0.8 shared electron pairs between any two adjacent Au atoms. The diagonal delocalization is approximately 0.2 electron pairs, which is not negligible, being close to the degree of sharing between two *para*-carbons in benzene. All these features support the notion that Au_4^{2-} exhibits a degree of σ–aromaticity.

The Cu_4 cluster is special in its response to the addition of an electron pair as the charge transfer between the two types of copper atoms increases by almost an order of magnitude. Thus, instead of a difference of 0.368 electronic charge between Cu1 and Cu2 in Cu_4, this difference is 1.085 in Cu_4^{2-}. In other words, *the entire 2e charge* gained by the cluster is distributed only between the two Cu2 atoms, those atoms that do not share the diagonal bond path. In the meantime, the two Cu1 atoms become virtually neutral in the double anion.

There exists a topological feature that distinguishes the doubly anionic copper cluster from its silver and gold counterparts. In the Cu_4^{2-} cluster, two non-nuclear attractors are found in the outer diffuse region of the electron density and these are shown in Fig. 5. Each NNA basin shares a zero-flux surface and a bond path with two Cu2 atoms and contains a population of 0.037 electrons. Figure 5 also shows the complete molecular graph of the Cu_4^{2-} cluster, which satisfies the PH relationship, Eq. (1). The bond properties of the bond path linking Cu2...NNA all have magnitude of 0.000 au, the first significant figure of each appearing in the fourth decimal, are hence not listed in Table 3.

The addition of two sodium ions to the M_4^{2-} clusters, to obtain the electrically-neutral composite clusters M_4Na_2, has a different effect depending on the nature of the metal. In the case of copper, the addition of the sodium ions can be described as "the great equalizer", since the highly polarized bonds in Cu_4^{2-} ($^{+0.068}$Cu1–Cu2$^{-1.017}$) are now between identical atom types in Cu_4Na_2, each with the intermediate charge of –0.442 a.u. In other words, the composite cluster is highly polarized, but equally and in opposite direction perpendicularly on the plane of the Cu_4 square. The copper atoms together bear a charge of –1.768 a.u., not much different than the –2

a.u of the Cu_4^{2-} cluster. The considerable charge redistribution must, then, be caused by the "ligand field" of the nearly spherical sodium atoms (as can be seen from the nearly spherical Na basins in the top part of the lowest panel in Fig. 4). Each Na atom bears almost an atomic unit of positive charge (q(Na) = +0.884 a.u.). An interesting feature of the bonding in Cu_4Na_2 is that ρ_{BCP} is slightly lower than in Cu_4^{2-} (0.055 a.u., and 0.058 a.u., respectively), yet there is an increase in electron sharing in the composite cluster between adjacent atoms from 0.675 pairs in Cu_4^{2-} to 0.730 in Cu_4Na_2. The lower density is accompanied by a lower magnitude of H_{BCP} and a slight bond elongation, all indicators of a slight weakening in the bonding at the expense of more even electron delocalization. Hence, it would be reasonable to predict that the Cu_4 skeleton in Cu_4Na_2 is more aromatic than that in Cu_4^{2-}. For silver and gold, a similar weakening of the peripheral M–M bonds is also encountered in M_4Na_2 compared to M_4^{2-} but, this time, with an accompanying slight decrease in electron delocalization between adjacent coinage metal atoms.

For all M_4Na_2, the charge on one of the two sodium atoms is close to unity, ranging from +0.88 in both the copper and silver composite clusters to +0.90 in the gold composite cluster. The $^{+0.90}Na–M^{-0.45}$ bonds are, therefore, characterized by considerable charge transfer across the zero-flux surface separating a sodium atom from a coinage metal atom (charge transfer of a magnitude ~ 1.4 a.u., to one decimal). Thus, there is a significant ionicity of the M-Na bond. This is well reflected in the very low delocalization indices characterizing these bonds since there is complete transfer of charge without delocalization. Thus, the δ(M,Na) is 0.072, 0.070, and 0.064 for M = Cu, Ag, and Au, respectively. Furthermore, the Na–M bonds are characterized by very small magnitudes and positive signs of H_{BCP}, in contrast to all metal-metal bonds between coinage metal atoms.

CONCLUSIONS

In conclusion, for the coinage metals, copper, silver and gold, all metal-metal bonds exhibit a dominance of the positive curvature (λ_3) and hence all exhibit positive $\nabla^2\rho_{BCP}$ values, a characteristic of closed-shell interactions. Thus, as other authors have noted, M–M bonding is ambiguous in the sense that it does not clearly fall into one or the other categories, these categories being too narrow to capture the richness and diversity of the bonding that can be quantitatively and unambiguously described by QTAIM atomic and bond properties.

For all M_2 clusters we identified linear correlations between the metal-metal bond strength and i) the ρ_{BCP} value, ii) the H_{BCP} value and iii) the values of the two principle negative curvatures at the bond critical point. Calculated QTAIM bond descriptors (ρ_{BCP}, H_{BCP} and $\delta(\Omega,\Omega')$ indicate that the M_4 metal-metal bonds are weaker than in the corresponding M_2 clusters. In general, peripheral M1-M2 bonds in M_4 clusters are moderately weaker than the diagonal M1-M1 bonds. Upon addition of an electron pair to the M_4 cluster, the diagonal M1-M1 bond weakens from copper to gold. The situation is somewhat different in the Au_4^{2-} cluster. Here the excess charge is distributed evenly between all Au atomic basins and the Au_4^{2-} cluster exhibits some degree of σ–aromaticity. In contrast, all excess electronic charge in the Cu_4^{2-} cluster is accumulated in the two non-bonded Cu basins. Addition of two sodium ions to each M_4^{2-} coinage metal cluster induces significant geometrical changes in M_4^{2-} (particularly for Cu and Ag) and results in a square rearrangement of the metal centers in all M_4Na_2 clusters. The M-M bond in the M_4Na_2 clusters is weaker than in the M_4^{2-} clusters, as predicted by QTAIM bond descriptors, and the M-Na bonds in the M_4Na_2 clusters are predominantly ionic.

It is fitting to end this paper with a 1952 quote from E. B. Wilson Jr., which underscores the importance of forgoing attempts to incarcerate nature into our narrow linguistic categories:[67]

> *"A class must be defined in terms of observable properties, and this often introduces difficulties of two kinds. The first difficulty is associated with the fact that most properties can vary continuously, at least from a practical viewpoint, so that clean-cut separations of things are often somewhat arbitrary .... The other difficulty concerns the fact that it is often necessary to amend definitions many times in order that the class may continue to be useful".*

ACKNOWLEDGEMENTS

The authors thank Dr. Todd A. Keith for drawing their attention to the existence of the non-nuclear attractor in the Cu_4^{2-} cluster and for very helpful discussions. The authors also thank Professor Kirk Peterson and Professor Markus Reiher for valuable comments and suggestions. This research has been supported by funding from a *Hong Kong UGC Special Equipment Grant* (SEG HKU09) and GRF HKU 702608P, *Natural Sciences and Engineering Research Council of Canada* (NSERC), *Canada Foundation for Innovation* (CFI), and an internal research grant from *Mount Saint Vincent University*.

References

1. Szabo, A.; Ostlund, N. S. *Modern Quantum Chemistry: Introduction to Advanced Electronic Structure Theory*; Dover Publications, Inc.: New York, 1989.
2. Levine, I. N. *Quantum Chemistry, (Sixth Edition)*; Pearson Prentice Hall: Upper Saddle River, New Jersey, 2009.
3. Parr, R. G.; Yang, W. *Density-Functional Theory of Atoms and Molecules*; Oxford University Press: Oxford, 1989.
4. Koch, W.; Holthausen, M. C. *A Chemist's Guide to Density Functional Theory, (Second Edition)*; Wiley-VCH: New York, 2001.
5. Dirac, P. A. M. *The Principles of Quantum Mechanics, Third Edition*; Oxford University Press: Oxford, 1958.
6. Bader, R. F. W.; Zou, P. F. *Chem. Phys. Lett.* **1992**, *191*, 54-58.
7. Coppens, P. *X-ray Charge Densities and Chemical Bonding*; Oxford University Press, Inc.: New York, 1997.
8. Hansen, N. K.; Coppens, P. *Acta Cryst. A* **1978**, *34*, 909-921.
9. Koritsanszky, T. S.; Coppens, P. *Chem. Rev.* **2001**, *101*, 1583-1628.
10. Bader, R. F. W. *Atoms in Molecules: A Quantum Theory*; Oxford University Press: Oxford, U.K., 1990.
11. Bader, R. F. W. *Monatsh. Chem.* **2005**, *136*, 819-854.
12. Bader, R. F. W. *Chem. Rev.* **1991**, *91*, 893-928.
13. Cortés-Guzmán, F.; Bader, R. F. W. *Coord. Chem. Rev.* **2005**, *249*, 633-662.
14. Popelier, P. L. A. *Atoms in Molecules: An Introduction*; Prentice Hall: London, 2000.
15. Matta, C. F.; Boyd, R. J. (Eds.) *The Quantum Theory of Atoms in Molecules: From Solid State to DNA and Drug Design*; Wiley-VCH: Weinheim, 2007.
16. Gervasio, G.; Bianchi, R.; Marabello, D. *Chem. Phys. Lett.* **2004**, *387*, 481-484.
17. Macchi P. ; Sironi, A. Chapter 13 in: *The Quantum Theory of Atoms in Molecules: From Solid State to DNA and Drug Design*; Matta, C. F.; Boyd, R. J. (Eds.), Wiley-VCH: Weinheim, 2007. pp. 345-374.
18. Macchi, P.; Garlaschelli, L.; Sironi, A. *J. Am. Chem. Soc.* **2002**, *124*, 14173-14184.
19. Farrugia, L. J.; Mallinsona, P. R.; Stewart, B. *Acta Cryst. B* **2003**, *59*, 234–247.
20. Macchioni, A. *Chem. Rev.* **2005**, *105*, 2039.
21. Macchi, P.; Sironi, A. *Coord. Chem. Rev.* **2003**, *238-239*, 383-412.
22. Macchi, P.; Proserpio, D. M.; Sironi, A. *J. Am. Chem. Soc.* **1998**, *120*, 13429-13435.
23. Gatti, C. *Z. Kristallogr.* **2005**, *220*, 399-457.
24. Gatti, C. ; Fantucci, P.; Pacchioni, G. *Theor. Chem. Acc. (Formerly, Theoret. Chim. Acta)* **1987**, *72*, 433-458.
25. Cao, W. L.; Gatti, C.; MacDougall, P. J.; Bader, R. F. W. *Chem. Phys. Lett.* **1987**, *141*, 380-385.
26. Sagar, R. P.; Ku, A. C. T.; Smith, V. H. Jr.; Simas, A. M. *J. Chem. Phys.* **1988**, *88*, 4367-4374.
27. Shi, Z.; Boyd, R. J. *J. Chem. Phys.* **1988**, *88*, 4375-4377.
28. Silvi, B. ; Gatti, C. *J. Phys. Chem. A* **2000**, *104*, 947-953 .
29. Aray, Y.; Rodriguez, J.; Vega, D. *J. Phys. Chem. B* **2000**, *104*, 4608-4612.

30. Mori-Sanchez, P.; Matin-Pendás, A.; Luaña, V. *J. Am. Chem. Soc.* **2002**, *124*, 14721-14723.
31. Bianchi, R.; Gervasio, G.; Marabello, D. *Inorg. Chem.* **2000**, *39*, 2360-2366.
32. Farrugia, L. J.; Middlemiss, D. S.; Sillanpää, R.; Seppälä, P. *J. Phys. Chem. A* **2008**, *112*, 9050-9067.
33. Bouhmaida, N.; Méndez-Rojas, M. A.; Pérez-Benitez, A.; Merino, G.; Fraisse, B.; Ghermani, N. E. *Inorg. Chem.* **2010**, *49*, 6443-6452.
34. Banerjee, A.; Singh, R.; Mondal, P.; Colacio, E.; Rajak, K. K. *Eur. J. Inorg. Chem.* **2010**, *5*, 790-798.
35. Pyykkö, P. *Angew. Chem. Int. Ed.* **2004**, *43*, 4412-4456.
36. Pyykkö, P. *Inorg. Chim. Acta* **2005**, *358*, 4113-4130.
37. Pyykkö, P. *Chem. Soc. Rev.* **2008**, *37*, 1967-1997.
38. Wannere, C. S.; Corminboeuf, C.; Wang, Z. X.; Wodrich, M. D.; King, R. B.; Schleyer, P. v. R. *J. Am. Chem. Soc.* **2005**, *127*, 5701-5705.
39. Lin, Y.-C.; Sundholm, D.; Jusélius, J.; Cui, L.-F.; Li, X.; Zhai, H.-J.; Wang, L.-S. *J. Phys. Chem. A* **2006**, *110*, 4244-4250.
40. Peterson, K. A.; Puzzarini, C. *Theor. Chem. Acc.* **2005**, *114*, 283-296.
41. Balasubramanian, K. *J. Mol. Struct. THEOCHEM* **1989**, *202*, 291-313.
42. Bauschlicher, J. C. W.; Langhoff, S. R.; Partridge, H. *J. Chem. Phys.* **1990**, *93*, 8133-8137.
43. Balasubramanian, K.; Feng, P. Y. *J. Phys. Chem.* **1990**, *94*, 1536-1544.
44. Lee, H. M.; Ge, M.; Sahu, B. R.; Tarakeshwar, P.; Kim, K. S. *J. Phys. Chem. B* **2003**, *107*, 9994-10005.
45. Assadollahzadeh, B.; Schwerdtfeger, P. *J. Chem. Phys.* **2009**, *131*, 064306-064311.
46. Prascher, B.; Woon, D.; Peterson, K.; Dunning, T.; Wilson, A. *Theoret. Chem. Acc. (Theoret. Chim. Acta)* **2011**, *128*, 69-82.
47. Handy N. C.; Schaefer III, H. F. *J. Chem. Phys., 81 (1984) 5031-33* **1984**, *81*, 5031-5033.
48. Wiberg, K. B.; Hadad, C. M.; LePage, T. J.; Breneman, C. M.; Frisch, M. J. *J. Phys. Chem., 96 (1992) 671-79* **1992**, *96*, 671-679.
49. Keith, T. A.; Frisch, M. J. *Private communication (manuscript submitted for publication)* **2011**.
50. Frisch, M. J.; Trucks, G. W.; Schlegel, H. B.; Scuseria, G. E.; Robb, M. A.; Cheeseman, J. R.; Scalmani, G.; Barone, V.; Mennucci, B.; Petersson, G. A.; Nakatsuji, H.; Caricato, M.; Li, X.; Hratchian, H. P.; Izmaylov, A. F.; Bloino, J.; Zheng, G.; Sonnenberg, J. L.; Hada, M.; Ehara, M.; Toyota, K.; Fukuda, R.; Hasegawa, J.; Ishida, M.; Nakajima, T.; Honda, Y.; Kitao, O.; Nakai, H.; Vreven, T.; Montgomery Jr, J. A.; Peralta, J. E. ; Ogliaro, F.; Bearpark, M.; Heyd, J. J. ; Brothers, E.; Kudin, K. N.; Staroverov, V. N.; Keith, T.; Kobayashi, R.; Normand, J.; Raghavachari, K.; Rendell, A.; Burant, J. C.; Iyengar, S. S.; Tomasi, J.; Cossi, M.; Rega, N.; Millam, J. M.; Klene, M.; Knox, J. E.; Cross, J. B.; Bakken, V.; Adamo, C.; Jaramillo, J.; Gomperts, R.; Stratmann, R. E.; Yazyev, O.; Austin, A. J.; Cammi, R.; Pomelli, C.; Ochterski, J. W.; Martin, R. L.; Morokuma, K.; Zakrzewski, V. G.; Voth, G. A.; Salvador, P.; Dannenberg, J. J.; Dapprich, S.; Daniels, A. D.; Farkas, O.; Foresman, J. B.; Ortiz, J. V.; Cioslowski, J.; Fox, D. J., *Gaussian 09, Revision B.01* (Gaussian Inc., Wallingford CT, 2010).
51. Keith, T. A., AIMAll (Version 09.02.01), aim@tkgristmill.com, 2009.

52. Nigam S.; Majumder, C. (Eds.) *Aromaticity and Metal Clusters*; CRC Press: New York, 2011.
53. Jiao, H.; Schleyer, P. v. R.; Mo, Y.; McAllister, M. A.; Tidwell, T. T. *J. Am. Chem. Soc.* **1997**, *119*, 7075-7083.
54. Schleyer, P.v-R.; Manoharan, M.; Wang, Z.-X.; Kiran, B.; Jiao, H.; Puchta, R.; Hommes, N. J. R. v. E. *Org. Lett.* **2001**, *3*, 2465-2468.
55. Chen, Z.; Wannere, C. S.; Corminboeuf, C.; Puchta, R.; Schleyer, P. v. R. *Chem. Rev.* **2005**, *105*, 3842-3888.
56. Schleyer, P.v-R.; Maerker, C.; Dransfeld, A.; Jiao, H.; Hommes, N. J. R. v. E. *J. Am. Chem. Soc.* **1996**, *118*, 6317-6318.
57. Keith, T. A.; Bader, R. F. W. *Chem. Phys. Lett.* **1992**, *194*, 1-8.
58. Keith, T. A.; Bader, R. F. W. *Chem. Phys. Lett.* **1993**, *210*, 223-231.
59. Bader, R. F. W.; Keith, T. A. *J. Chem. Phys.* **1993**, *99*, 3683-3693.
60. Keith, T. A.; Bader, R. F. W. *J. Chem. Phys.* **1993**, *99*, 3669-3682.
61. Keith, T. A.; Bader, R. F. W. *Int. J. Quantum Chem.* **1996**, *60*, 373-379.
62. Pauling, L. *The Nature of the Chemical Bond, (Third Ed.)*; Cornell University Press: Ithaca, N.Y., 1960.
63. Luo, Y.-R. *Handbook of Bond Dissociation Energies in Organic Compounds*; CRC Press: New York, 2003 .
64. Matta, C. F.; Hernández-Trujillo, J. *J. Phys. Chem. A* **2003**, *107*, 7496-7504 (Correction: J. Phys. Chem A, **2005**, *109*, 10798).
65. Espinosa, E.; Molins, E.; Lecomte, C. *Chem. Phys. Lett.* **1998**, *285*, 170-173.
66. Fradera, X.; Austen, M. A.; Bader, R. F. W. *J. Phys. Chem. A* **1999**, *103*, 304-314.
67. Wilson, E. B. *An Introduction to Scientific Research*; McGraw-Hill Book Co., Inc.: New York, 1952.
68. Ram, R. S.; Jarman, C. N.; Bernath, P. F. *J. Mol. Spectr.* **1992**, *156*, 468-486.
69. Rohlfing, E. A.; Valentini, J. J. *J. Chem. Phys.* **1986**, *84*, 6560-6566.
70. Ran, O.; Schmude, Jr. R. W.; Gingerich, K. A.; Wilhitef, D. W.; Kingcade, Jr. J. E. *J. Phys. Chem.* **1993**, *97*, 8535-8540.
71. Huber, K. P.; Herzberg, G. *Molecular spectra and molecular structure IV. Constants of Diatomic molecules* ; Van Nostrand: Princeton, 1979.
72. James, A. M.; Kowalczyk, P.; Simard, B.; Pinegar, J. C.; Morse, M. D. *J. Mol. Spect.* **1994**, *168*, 248-257.

Table 1 Chemical formulae, total charges, point group symmetries, and total energies of the coinage metal clusters.[(a)]

Chemical Formula	Total Charge	Point Group Symmetry	Total Energy (a.u.)	Total Energy Including ZPE Correction (a.u.)	Total Binding Energy[(b)] (kcal/mol)	Binding Energy per Atom[(b)] (kcal/mol)
Cu_2	0	$D_{\infty h}$	-393.48631	-393.48567	-46.1(-46.5)	-23.1(-23.3)
Cu_4	0	D_{2h}	-787.04164	-787.03915	-134.7(-136.2)	-33.7(-34.1)
Cu_4^{2-}	-2	D_{2h}	-786.99178	-786.98954	-103.5(-104.9)	-25.9(-26.2)
Cu_4Na_2	0	D_{4h}	-1110.85952	-1110.85532	[(c)]	[(c)]
Ag_2	0	$D_{\infty h}$	-293.00101	-293.00053	-41.1(-41.4)	-20.6(-20.7)
Ag_4	0	D_{2h}	-586.06074	-586.05900	-118.5(-119.6)	-29.6(-29.9)
Ag_4^{2-}	-2	D_{2h}	-586.03265	-586.03116	-101.0(-101.9)	-25.3(-25.5)
Ag_4Na_2	0	D_{4h}	-909.89167	-909.88829	[(c)]	[(c)]
Au_2	0	$D_{\infty h}$	-270.44252	-270.44206	-56.5(-56.8)	-28.3(-28.4)
Au_4	0	D_{2h}	-540.96080	-540.95920	-160.2(-161.2)	-40.1(-40.3)
Au_4^{2-}	-2	D_{4h}	-540.99419	-540.99280	-181.3(-182.2)	-45.3(-45.6)
Au_4Na_2	0	D_{4h}	-864.87280	-864.86947	[(c)]	[(c)]

(a) In the calculations of binding energies, the ground state of all free atoms is $^2S_{1/2}$, and of all dimers is $\boldsymbol{X}^1\Sigma_{\boldsymbol{g}}^+$.

(b) The energies of the free ground state atoms used to calculate the binding energies are the result of restricted-open shell (RO) calculations, that is, RO–MP2(FC)/aug-cc-pVTZ-PP(*spdfg*). The listed binding energies include the zero-point vibrational energy corrections (ZPE), and thus comparable to experimental values extrapolated to the absolute zero of temperature. Values in brackets are the binding energies without the ZPE corrections.

(c) The frozen core (FC) MP2 energy for Na^+ is zero since it lacks valence electrons. Therefore, we did not calculate the MP2 binding energies of the M_4Na_2 clusters.

Table 2 Comparison of experimental and calculated bond dissociation energies (BDE) and bond lengths (BL) of the coinage metal dimers M_2 (M = Cu, Ag, Au).[(a-c)]

	Cu_2	Ag_2	Au_2
BDE (0K) *Expt.* (kcal/mol)	47.9±0.6	37.8±0.8	53.2±0.1
BDE (0K) *Calc.* (kcal/mol)	46.1(46.5)	41.1(41.4)	56.5(56.8)
BL *Expt.* (Å)	2.219	2.530	2.472
BL *Calc.* (Å)	2.198	2.492	2.451
Refs. for Expt. values	BL,[68] BDE[69]	BL,[70] BDE[70]	BL,[71] BDE[72]

(a) The ground state of all free atoms is $^2S_{1/2}$, and of all dimers is $\boldsymbol{X}\,^1\Sigma_{\boldsymbol{g}}^+$.

(b) Experimental uncertainties are at a decimal beyond the third for the experimental bond lengths and hence are omitted.

(c) The energies of the free ground state atoms used to calculate the BDEs are the result of restricted-open shell (RO) calculations, that is, RO–MP2(FC)/aug-cc-pVTZ-PP(*spdfg*). BDE calculations include the zero-point vibrational energy corrections (ZPE), and thus are directly comparable to the reported experimental values extrapolated to the absolute zero of temperature. Values in brackets are the BDEs without the ZPE corrections).

Table 3 Selected Bond Properties[a,b,c]

Cluster/ Interaction[d]	Distance (Å)[d]	DI δ(A,B)	ρ_{BCP}	$\nabla^2\rho_{BCP}$	λ_1	λ_2	λ_3	ε	V_{BCP}	G_{BCP}	H_{BCP}
Cu_2											
Cu–Cu	2.198	1.152	0.073	0.152	–0.068	–0.068	0.289	0.000	–0.094	0.066	–0.028
Cu_4											
Cu1–Cu1	2.214	0.564	0.069	0.164	–0.067	–0.051	0.282	0.307	–0.091	0.066	–0.025
Cu1–Cu2	2.344	0.622	0.058	0.096	–0.048	–0.035	0.179	0.390	–0.064	0.044	–0.020
Cu2...Cu2	4.132	0.148									
Cu_4^{2-}											
Cu1–Cu1	2.417	0.591	0.070	0.160	–0.066	–0.050	0.276	0.327	–0.092	0.066	–0.026
Cu1–Cu2	2.326	0.675	0.058	0.095	–0.048	–0.035	0.178	0.400	–0.064	0.044	–0.020
Cu2...Cu2	3.975	0.498									
Cu_4Na_2											
Cu–Cu	2.355	0.730	0.055	0.096	–0.044	–0.041	0.182	0.070	–0.061	0.043	–0.019
Cu–Na	2.812	0.072	0.013	0.054	–0.005	–0.003	0.061	0.820	–0.010	0.012	0.002
Cu...Cu	3.331	0.209									
Na...Na	4.531	0.002									
Ag_2											
Ag–Ag	2.492	1.081	0.064	0.179	–0.055	–0.055	0.289	0.000	–0.082	0.063	–0.019
Ag_4											
Ag1–Ag1	2.544	0.513	0.056	0.166	–0.049	–0.042	0.257	0.163	–0.070	0.056	–0.014
Ag1–Ag2	2.650	0.555	0.048	0.121	–0.037	–0.032	0.189	0.179	–0.052	0.041	–0.011
Ag2...Ag2	4.650	0.146									
Ag_4^{2-}											
Ag1–Ag1	2.936	0.454	0.029	0.068	–0.019	–0.009	0.095	1.198	–0.023	0.020	–0.003
Ag1–Ag2	2.632	0.687	0.048	0.130	–0.038	–0.036	0.205	0.064	–0.054	0.043	–0.011
Ag2...Ag2	4.370	0.205									
Ag_4Na_2											
Ag–Ag	2.689	0.634	0.045	0.111	–0.033	–0.031	0.175	0.064	–0.047	0.037	–0.009
Ag–Na	2.944	0.070	0.012	0.048	–0.006	–0.004	0.058	0.589	–0.009	0.010	0.002
Ag...Ag	3.802	0.182									
Na...Na	4.496	0.002									
Au_2											
Au–Au	2.451	1.188	0.093	0.220	–0.087	–0.087	0.394	0.000	–0.130	0.093	–0.038
Au_4											
Au1–Au1	2.553	0.571	0.075	0.191	–0.067	–0.061	0.319	0.085	–0.098	0.073	–0.025

Cluster/ Interaction[(d)]	Distance (Å)[(d)]	DI δ(A,B)	ρ_{BCP}	$\nabla^2\rho_{BCP}$	λ_1	λ_2	λ_3	ε	V_{BCP}	G_{BCP}	H_{BCP}
Au2–Au1	2.607	0.691	0.069	0.164	–0.058	–0.053	0.276	0.091	–0.084	0.063	–0.022
Au2–Au2	4.547	0.157									
Au_4^{2-}											
Au–Au	2.606	0.799	0.069	0.165	–0.058	–0.058	0.281	0.004	–0.084	0.063	–0.021
Au...Au	3.685	0.199									
Au_4Na_2											
Au–Au	2.647	0.752	0.065	0.155	–0.051	–0.049	0.255	0.047	–0.076	0.058	–0.019
Au–Na	2.925	0.064	0.013	0.064	–0.008	–0.006	0.077	0.397	–0.011	0.014	0.002
Au...Au	3.743	0.175									
Na...Na	4.496	0.001									

(a) Dimensioned quantities are all in atomic units (a.u.) except distances which are in Angstroms (Å).
(b) Symmetry-unique interactions are listed once.
(c) The subscript BCP signifies that the value is reported at the "bond critical point"; δ(A,B) is the delocalization index between atoms A and B;[66] λ_n is the n^{th} curvature of the electron density at the BCP where by convention $|\lambda_1| \geq |\lambda_2|$; ε is the bond ellipticity defined by $\varepsilon = \lambda_1/\lambda_2 - 1$; and V_{BCP}, G_{BCP}, and H_{BCP} are the potential, gradient kinetic, and total energy densities at the BCP, respectively. ($H_{BCP} = V_{BCP} + G_{BCP}$).
(d) Distances are the geometrical bond length for bonds designated with a dash (–) and geometric distance in case of non-bonded interactions designated by dots (...). For the atom numbering scheme see Fig. 1.

Table 4 Selected Atomic Properties[a]

Cluster/ Atom[b]	$q(\Omega)$	$N(\Omega)$	LI $\Lambda(\Omega)$	Vol(Ω), 0.001 a.u.
Cu_2				
Cu	0.000	19.000	18.454	240.7
Sum	0.000	38.000	36.909	481.3
Cu_4				
Cu1	0.184	18.816	17.925	176.3
Cu2	-0.185	19.185	18.520	242.5
Sum	-0.001	76.001	72.891	837.6
Cu_4^{2-}				
Cu1	0.068	18.932	17.969	185.0
Cu2	-1.017	20.017	19.084	293.6
NNA[c]	-0.037	0.037	0.003	0.0
Sum	-1.971	77.971	74.112	957.3
Cu_4Na_2				
Cu	-0.442	19.442	18.561	256.6
Na	0.884	10.116	9.976	70.9
Sum	0.000	98.000	94.196	1168.3
Ag_2				
Ag	0.000	19.000	18.475	278.8
Sum	0.000	38.000	36.951	557.6
Ag_4				
Ag1	0.199	18.801	17.994	215.7
Ag2	-0.199	19.199	18.587	283.8
Sum	0.000	76.000	73.162	999.0
Ag_4^{2-}				
Ag1	-0.536	19.536	18.715	331.6
Ag2	-0.465	19.465	18.714	334.9
Sum	-2.002	78.002	74.858	1333.1
Ag_4Na_2				
Ag	-0.442	19.442	18.661	298.7
Na	0.883	10.117	9.977	71.4
Sum	0.000	98.000	94.597	1337.5

Cluster/ Atom[(b)]	$q(\Omega)$	$N(\Omega)$	LI $\Lambda(\Omega)$	Vol(Ω), 0.001 a.u.
Au_2				
Au	0.000	19.000	18.415	284.4
Sum	0.000	38.000	36.830	568.9
Au_4				
Au1	0.189	18.811	17.838	227.0
Au2	-0.189	19.189	18.429	282.8
Sum	0.000	76.000	72.533	1019.5
Au_4^{2-}				
Au	-0.503	79.503	18.627	327.5
Sum	-2.013	318.013	74.509	1310.1
Au_4Na_2				
Au	-0.452	19.452	18.561	291.9
Na	0.904	10.096	9.970	66.7
Sum	0.000	98.000	94.182	1300.8

(a) The atomic properties listed in this table are all in atomic units (a.u.) and include: the atomic charge q(Ω); the atomic electron populations (that only includes the electrons treated explicitly in the electronic structure calculation $N(\Omega)$; the localization index (LI) $\Lambda(\Omega)$;[66] the atomic volume enclosed by the zero-flux interatomic surface(s) bounding the atom within the cluster and the outer isodensity envelope of $\rho = 0.001$ a.u. that represents the outer van der Waals surface in the gas-phase[10] Vol(Ω) 0.001 a.u. Only symmetry-unique atoms are listed explicitly along with the molecular sums. For the atom numbering scheme see Fig. 1.

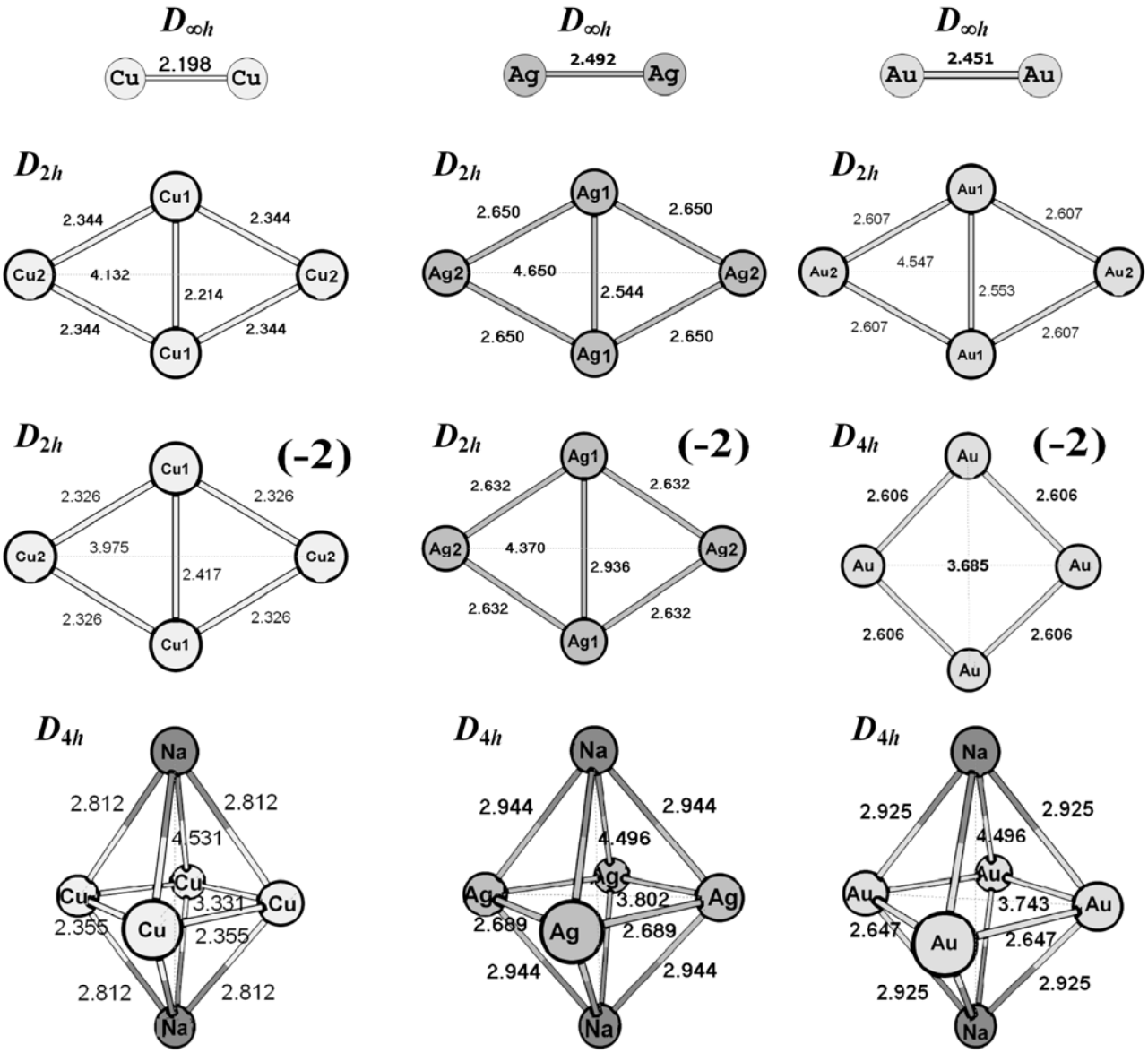

Fig. 1 Optimized molecular geometries of the 12 studied clusters. Some of the symmetry unique bond lengths and non-bonded distances are given in Å along with the point group symmetry of each cluster. All clusters are electrically neutral except the clusters in the third row, each of which carrying a total charge of –2 a.u. Each one of the 12 molecular structures is drawn to scale within itself, but the 12 different structures are not to scale with respect to one another.

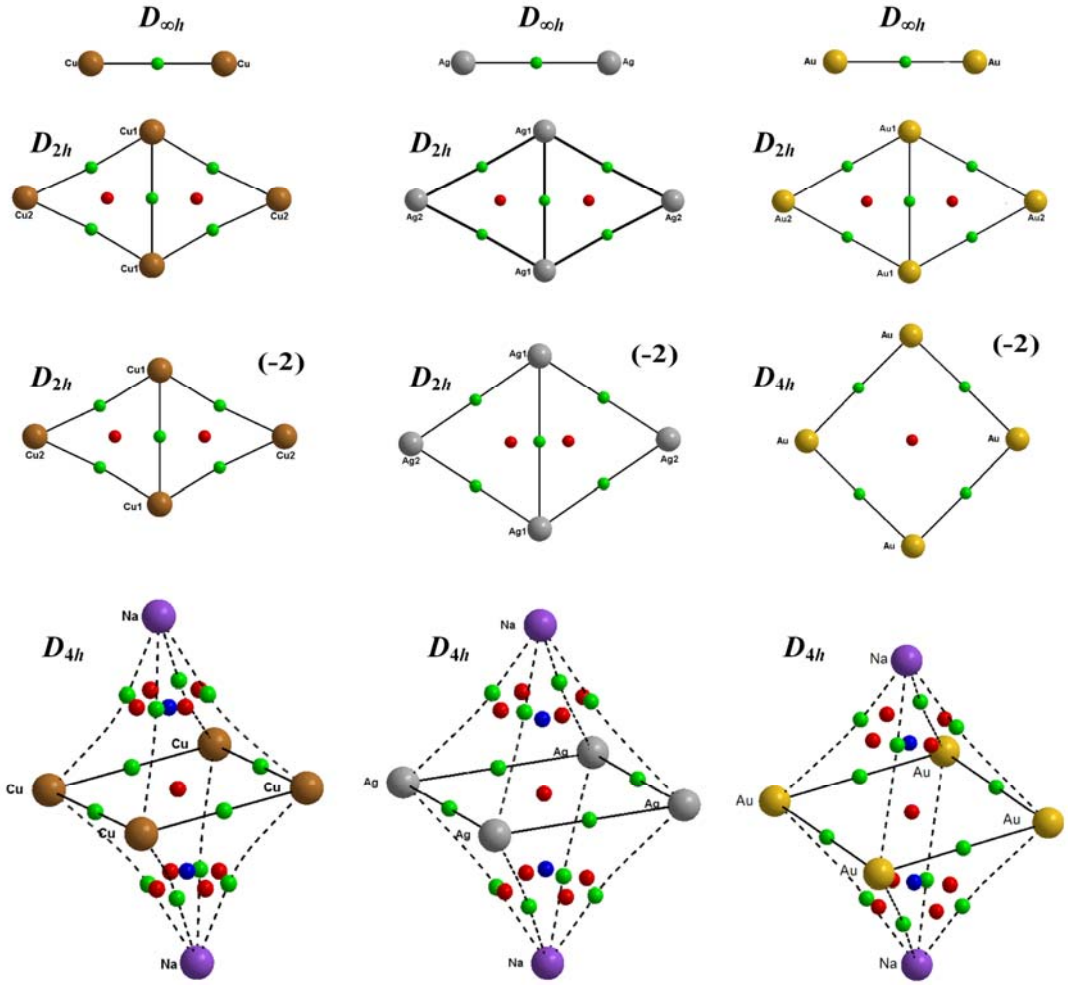

Fig. 2 Molecular graphs of the 12 studied clusters along with the point group symmetry of each cluster, in the same order and arrangement as in Fig. 2. The solid lines are bond paths characterized by a $\rho_{BCP} \geq 0.025$ a.u., i.e. what can be considered generally as a stronger bonding interaction, dotted bond path are characterized by $\rho_{BCP} < 0.025$ a.u. The atomic nuclear position is indicated by the large spheres, color coded by element: Cu = brown, Ag = grey, Au = golden yellow, and Na = violet. Critical points in the electron density are depicted by the smaller spheres, color coded: Bond critical points (BCP) = green, ring critical points (RCP) = red, and cage critical points (CCP) = dark blue. All molecular graphs depicted above are complete except that the graph of Cu_4^{2-} from which the non-nuclear attractors (NNA) have been omitted for clarity (See Fig. 5 for the complete graph of this complex). All clusters are electrically neutral except the clusters in the third row, each of which carrying a total charge of –2 a.u. Each one of the 12 molecular structures is drawn to scale within itself, but the 12 different structures are not to scale with respect to one another.

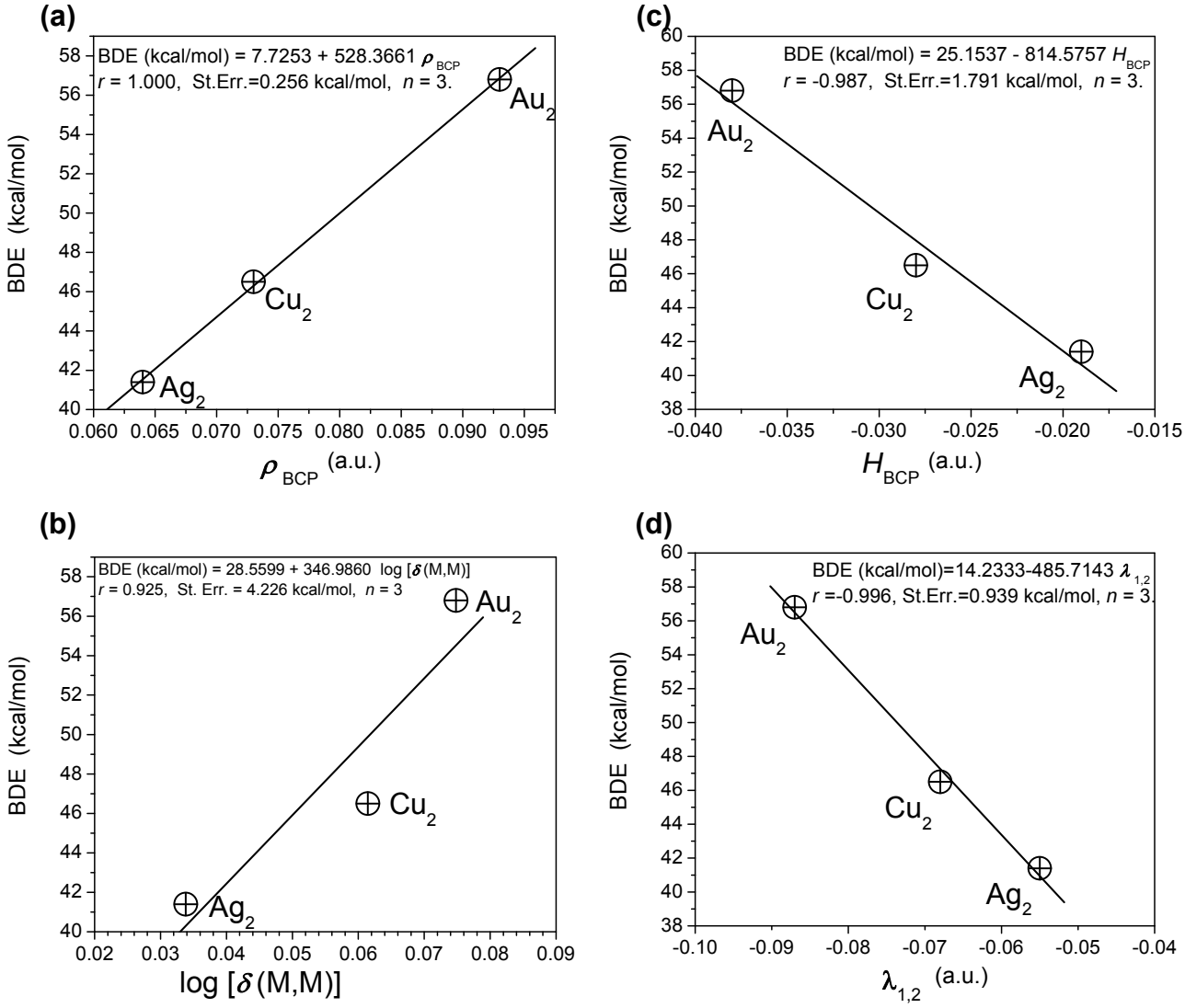

Fig. 3 Correlations between QTAIM bonding descriptors and the bond dissociation energy (without zero-point energy correction) of the diatomic clusters, M_2 (M = Cu, Ag, Au). (a) Correlation between ρ_{BCP} and BDE; (b) Correlation between log δ(M,M) and BDE; (c) Correlation between H_{BCP} and BDE; (d) Correlation between $\lambda_{1,2}$ and BDE.

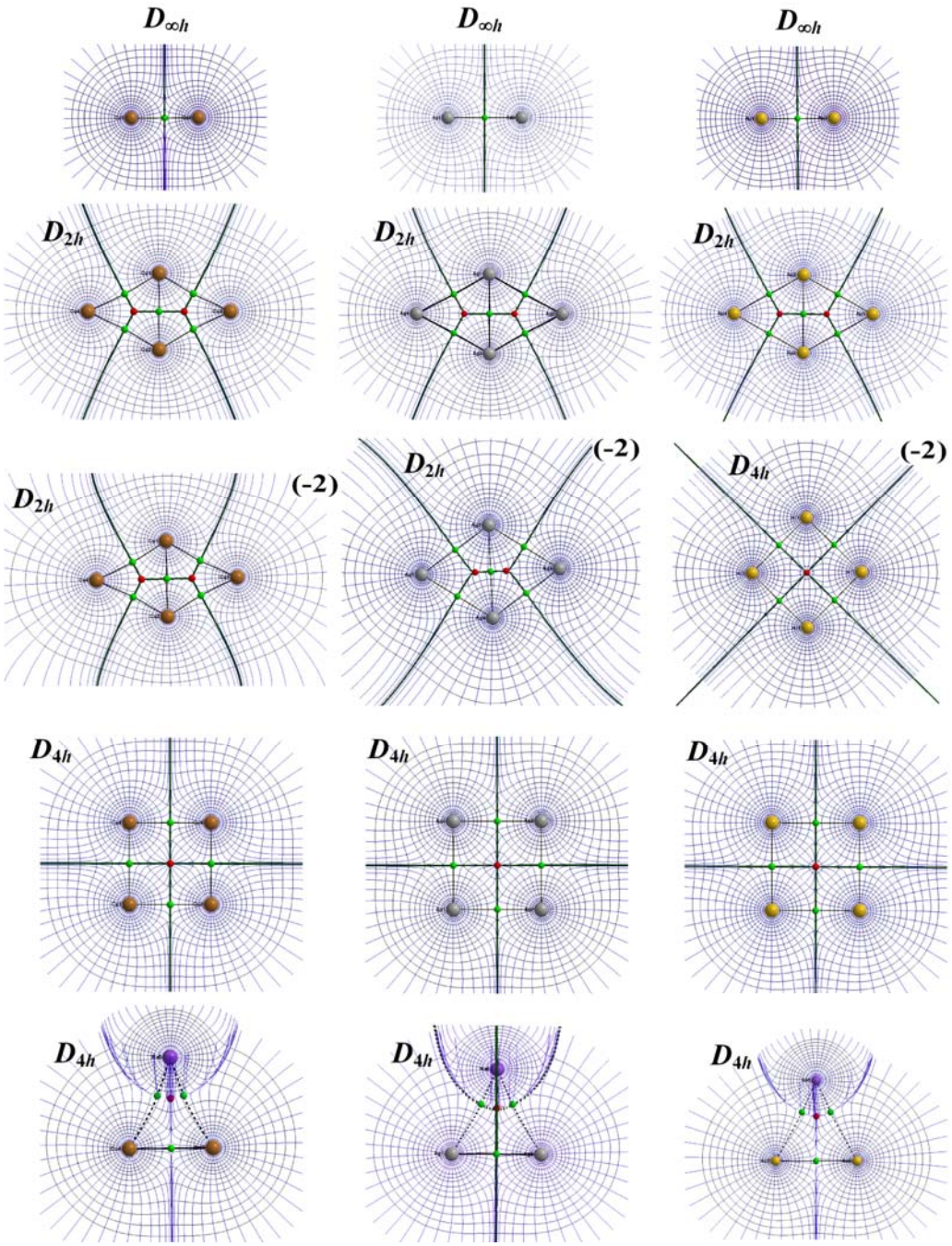

Fig. 4 Electron density contour lines and the associated gradient vector field in the planes of the nuclei of the coinage metal atoms (except the last panel, in the plane of two coinage and one Na atom) in the 12 studied clusters. The isodensity of ρ have the values (in a.u.): 0.001, 0.002 0.004 0.008 0.02, 0.04, 0.08, 0.2, 0.4, 0.8, 2.0, 4.0, 8.0, from the outer to inner contours. Superposed on each plot is the molecular graph (or portion of the molecular graph in the plane of the plots, in the case of the M_4Na_2 clusters, the two last panels). The color codes and convention regarding the molecular graph have been introduced in the caption of Fig. 2. The clusters are organized in the same arrangement as in Figs. 2 and 3, except for the addition of the M-M-Na plane in the bottom panel. All clusters are electrically neutral except the clusters in the third row, each of which carrying a total charge of –2 a.u. Each one of the 12 molecular structures is drawn to scale within itself, but the 12 different structures are not to scale with respect to one another.

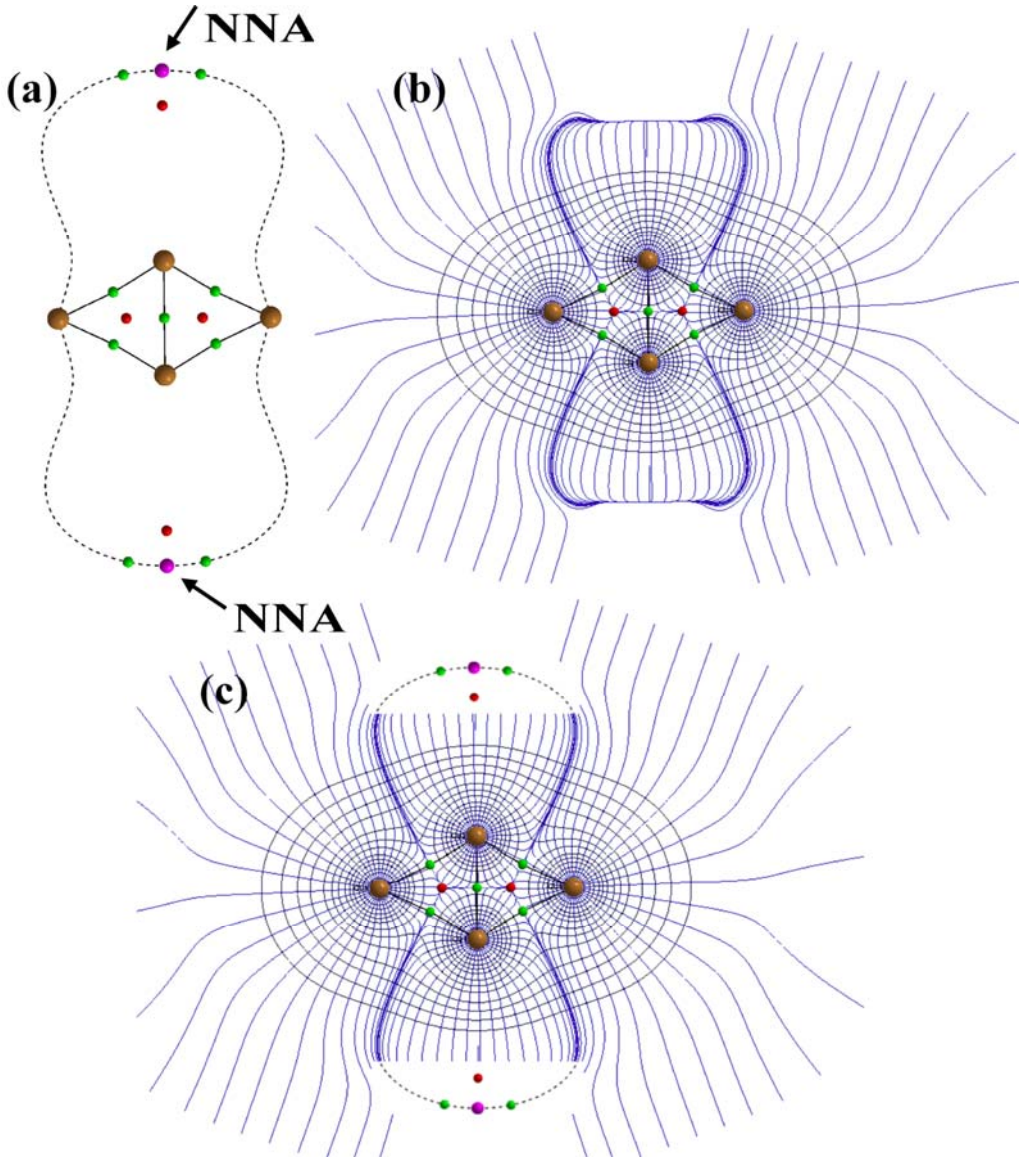

Fig. 5 (a) Complete molecular graph, and (b) electron density contours of Cu_4^{2-} and their associated gradient vector field extending to the region where the electron density of this anion is diffuse showing the position of the two nonnuclear attractors. Each electron attractor is 3.703 Å away from the nearest Cu1 atom. The plot in (c) combines parts of the molecular graph in (a) with the plot in (b). The same conventions as the previous figures (Figs. 3 and 4) are adopted in the above plots.